CONFERENCE PRE-PRINT

TITANIUM ADDITION AND THICKNESS VARIATION RESEARCH IN TUNGSTEN BLOCK BEHAVIOR AS FUSION PLASMA FACING FIRST WALL

A. ZALCMAN
Conicet & Instituto Sabato, Universidad Nacional de San Martín
Buenos Aires, Argentina
Email: alexiszalcman@gmail.com

J.L. GERVASONI
Cnea & Conicet
Bariloche, Argentina

Abstract

The objective of this study is to systematically evaluate the response of pure Tungsten and Tungsten-Titanium (W-Ti) alloys containing up to 4 wt.% Ti to a monoenergetic neutron flux of 14.1 MeV, representative of a deuterium-tritium (D-T) fusion plasma. The analysis focuses on the influence of alloy composition and structural wall thickness on key nuclear performance metrics, including neutron shielding efficacy, primary radiation-induced damage, transmutation-induced degradation, and neutron multiplication phenomena arising from (n,xn) reactions.

1. INTRODUCTION

The nuclear behavior of tungsten (W) under fission neutron spectra has been extensively characterized and validated [1]. Due to its exceptionally high melting point (~3700 K), outstanding mechanical strength, and superior physicochemical stability relative to other candidate materials, tungsten is considered one of the most promising options for the construction of divertor components and first wall shielding in tokamak-based fusion systems and fusion–fission hybrid reactors [2].

The primary role of the first wall is to shield the tritium breeding blanket (TBB) from energetic ions originating in the plasma, while simultaneously preserving the neutron economy essential for sustaining the lithium-based breeding reactions:

- Li-6(n, α + T), which is favored by thermal (low-energy) neutrons
- Li-7(n, α + T + n'), which exhibits peak cross-section efficiency within the intermediate energy range of approximately 5.5 to 10 MeV.

Multiple studies have shown that adding up to 4% by weight of Ti to W can improve its flexural strength and toughness, reduce the brittle-ductile transition temperature (the major deficit of pure W), improve resistance to embrittlement by irradiation, and help to maintain both the stability of nanometric structures at high temperatures, as well as to control the concentration range of embrittlement impurities such as H and He [3]. By adding an appropriate amount of Ti, it might be possible to suppress the clustering of Re and Os, thereby potentially improving the radiation resistance of tungsten materials for nuclear fusion applications [4- 6]. However, there is a lack of experimental information on the behavior of this material in real environments of neutron fusion irradiation (E=14Mev), and extrapolating the performance of W or W-xTi based on the available information on the response of the material to fission neutrons continues to raise doubts [7]. Therefore, simulation must be used to predict the material's behavior under conditions consistent with the environment generated in D-T nuclear fusion, as is the case in this work.

2. COMPUTATIONAL MODELING

Monte Carlo radiation transport simulations were conducted using the MCNP5 code (RSICC, V. 1.4) [8], configured to account exclusively for neutron interactions (MODE N) [9], [10].

The simulated geometry consists of a prismatic column with a 1 cm² square incident surface and variable thicknesses, designed to represent a section of the reactor's first wall. Periodic boundary conditions were applied laterally to emulate an infinite wall and eliminate neutron leakage artifacts.

Material compositions included pure tungsten and W–Ti alloys with titanium atomic fractions of x= {0, 2, 4}% . Alloys were treated as ideal mixtures for density calculations, comprising naturally occurring isotopes of tungsten (W-180, W-182, W-183, W-184, W-186) and titanium (Ti-46, Ti-47, Ti-48, Ti-49, Ti-50).

The neutron source was modelled as a monoenergetic flux of 14.1 MeV, representative of D–T fusion reactions in magnetic confinement devices or dense plasma focus (DPF) systems. Neutrons θ_0 were emitted uniformly from a planar source located 1 cm in front of the incidence surface, with a direction vector normal to the surface (see scheme below):

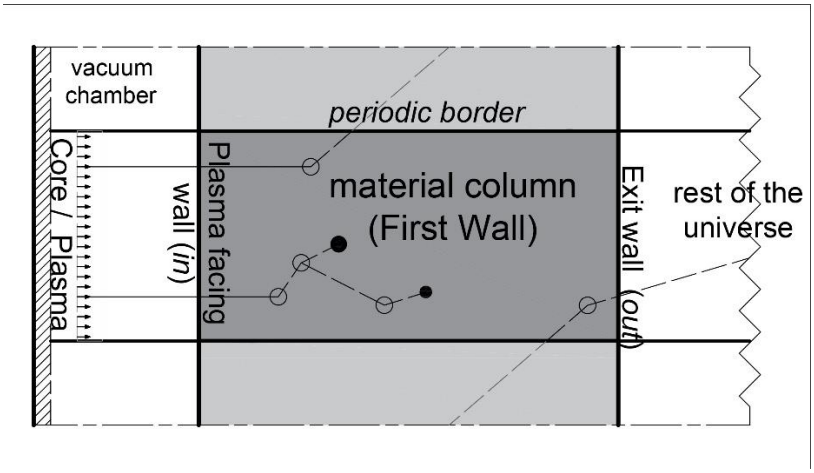

Simulation results were normalized based on either neutron flux. In the initial simulation series, the neutron shielding capability of the candidate materials under fusion-relevant conditions was quantitatively assessed. Key nuclear response parameters were extracted, including the scalar neutron flux within the wall volume (tally F4), the energy deposition profile (tally F6), the neutron current reflected back toward the reactor core, and the escaping neutron current through the rear surface (tallies F11 and F21). Additionally, the primary radiation-induced damage, expressed as displacements per atom (DPA), was evaluated using a flux tally F34 in conjunction with an FM34 modification card (1 1 444), resolved as a function of the incident particle energy.

Energy binning was performed using non-uniform intervals spanning from 0.5 eV to 20 MeV, enabling the computation of reaction-specific average energies as a function of material depth. The transmutation damage profile—arising from (n,γ) and (n,xn) reactions—was further characterized using an F14 neutron flux tally with an FM14 modifier card (-1 1 102)(-1 1 16:17), independent of the interacting particle energy spectrum.

To resolve spatial gradients, tally splitting cards (FS) were employed to segment the material column into subcells of 500 μm thickness for depths x ≤ 5 cm, and 5 mm for deeper regions. The transmutation damage was thus mapped as a depth-dependent function. The DPA rate, normalized to source particles, was calculated using the Norgertt-Robinson-Torrens (NRT) model, as defined by the following equation [8]:

$$\dot{D}_{x-P}(x) = \phi_0 \frac{\rho_a \eta}{2E_d} \sum_{\Delta E_i} F34_{Ei}(x) \quad (1)$$

Where ϕ_0 denotes the incident neutron flux (which may be transposed to the opposite side of the equation for normalization purposes), ρ_a represents the atomic density of the material, and the constants η (typically 0.8) and E_d (ranging between 70 and 90 eV) are material-dependent parameters obtained from tabulated data specific to the Norgertt-Robinson-Torrens (NRT) model [9]. The computed tally F34_Ei(x) is expressed in units of [MeV·barn/cm²].

The current standard NRT-DPA model is based on Binary Collision Approximation (BCA) calculation [11], therefore overestimates the real number of atomic displacements, spetialy for fast neutron spectrum, due to the

recombination of atoms before thermal equilibrium [12,13,14]. Konobeyev et al. addres this, proposing a new model that considers the athermal recombination correction (or ARC-DPA) since 2015 [14] and 2018 [15]. To correct the obtained DPA values, an approach already applied by S. Chen was used, applying a correction factor quotient of Konobeyev's ARC-DPA cross section over NRT-DPA dependent on the energy intervals [16]:

$$\dot{D}_{x-P}(x)\Big|^{corr} = \phi_0 \frac{\rho_a \eta}{2E_d} \sum_{\Delta E_i} \frac{\langle \sigma^{ARC} \rangle}{\langle \sigma^{NRT} \rangle}\Big|_{\Delta E} F34_{Ei}(x) \quad (2)$$

3. RESULTS AND DISCUSSION

To quantify key parameters that characterize titanium behaviour within tungsten—particularly radiation-induced damage—and to assess titanium's influence on primary damage mechanisms, molecular dynamics (MD) simulations will be employed. These simulations will be calibrated according to the methodology outlined in Equation (2).

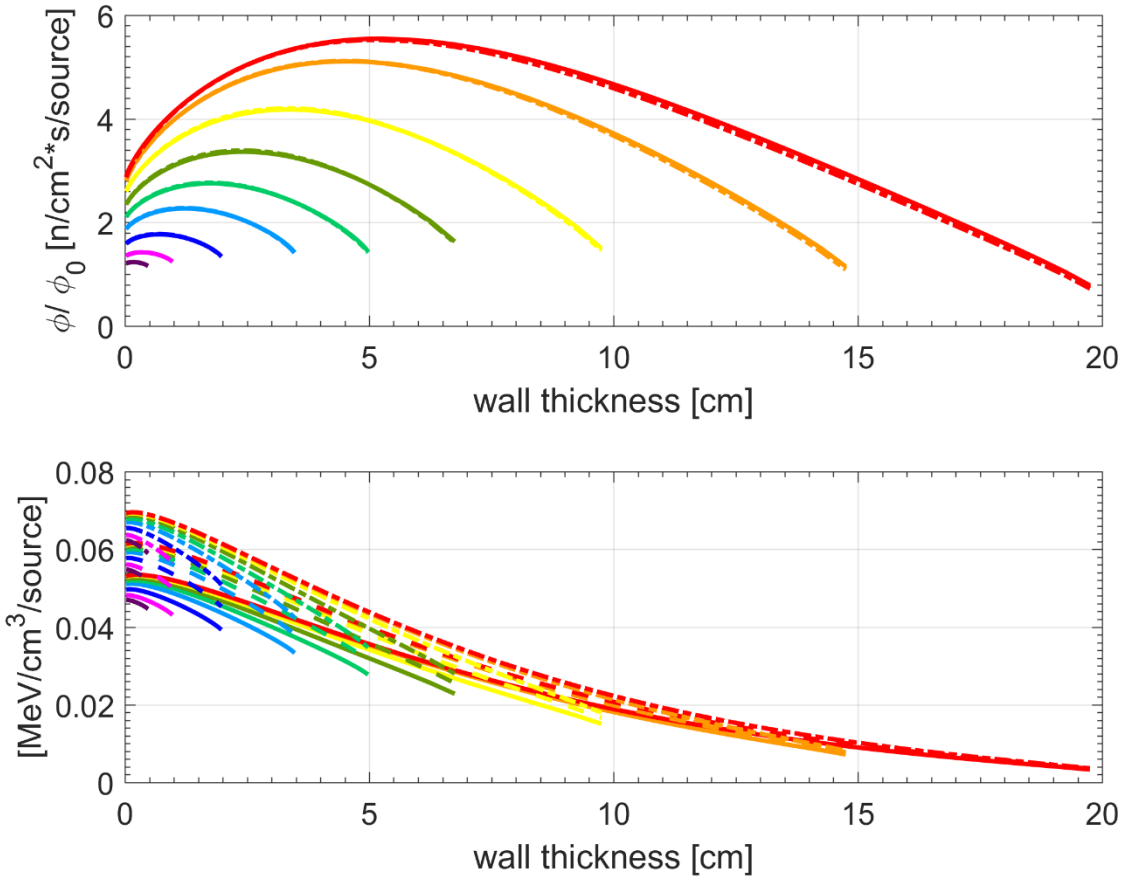

FIG. 1.: ***Top****: Ti ratio and thickness-dependent Neutron scalar flux profile normalized to incident flux inside the wall.* ***Bottom:*** *normalized Energy deposited rate profile inside the wall, evaluated as a function of the same variables. Solid line for pure W, dashed line for 2% Ti and dash-dot line for 4% Ti alloy.*

3.1. Neutron Scalar Flux

The variation in titanium content within the W-Ti alloy exhibits no significant impact on the scalar neutron flux distribution. Peak flux values occur at comparable depths across all compositions, with a maximum deviation of approximately 1% between pure tungsten (solid line) and the alloy containing 4 wt.% Ti (dash-dotted line, see FIG 1, Top). A characteristic flux amplification is observed in all cases, attributed to tungsten's (n,xn) secondary neutron production reactions, with the peak located at a normalized depth (x/d) between 31% and 36% of the total

wall thickness. Furthermore, an increase in wall thickness leads to a proportional rise in flux magnitude, following a linear trend.

3.2. Neutron-Induced Reaction Rates:

The variation in titanium content within the W-Ti alloy exhibits no discernible impact on the reaction rate profiles across all evaluated cases (FIG 2). The volumetric (n,xn) reaction rate appears largely insensitive to changes in wall thickness, except for a slight increase near the incident neutron surface, followed by a monotonic decline with depth. In contrast, the (n,γ) reaction rate displays a parabolic trend, increasing with wall thickness and peaking at approximately 40% of the total depth. Nevertheless, across the full range of studied thicknesses (0.5 to 20 cm), the (n,xn) reaction rate responsible for neutron multiplication consistently exceeds the absorption rate by a factor ranging from 4 to 100, indicating a net neutron multiplication effect throughout the material.

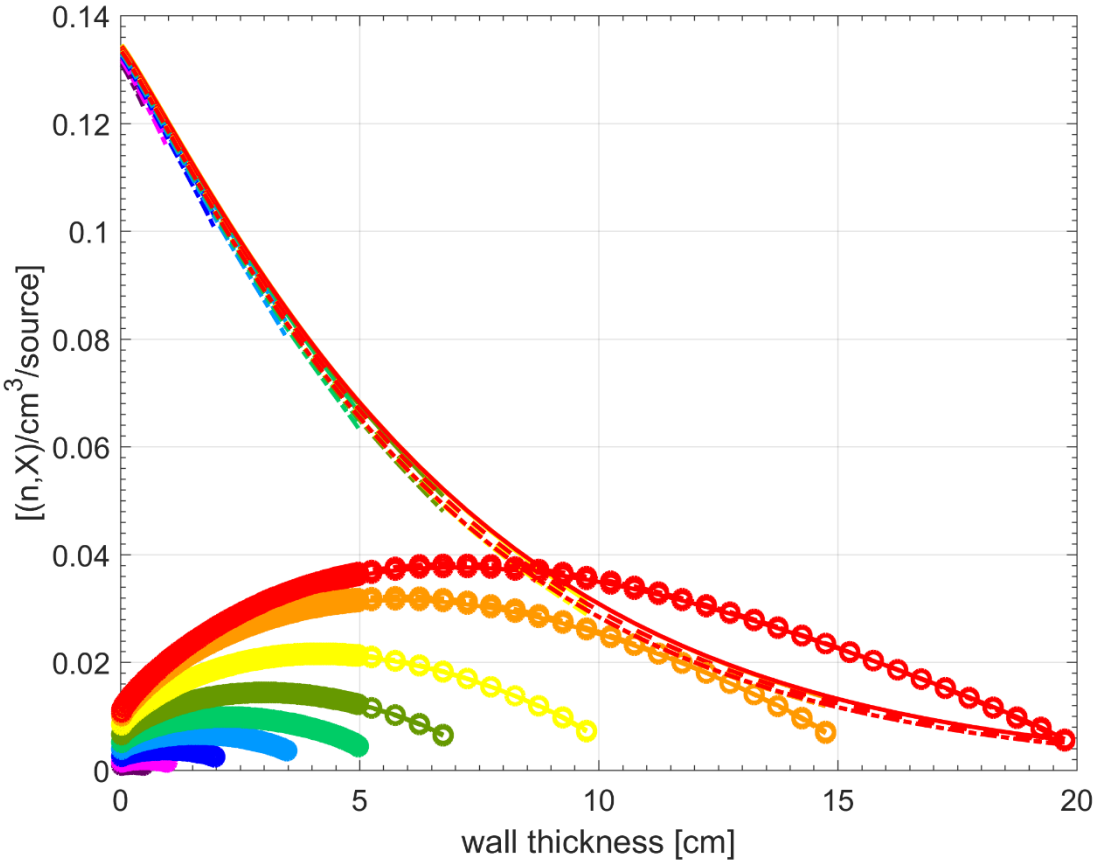

FIG. 2. ***Lined****: Net reaction rate profile (n,xn) normalized to incident flux inside the wall as a function of Ti proportion and thickness****. Circle marked:*** *Normalized absorption reaction rate profile inside the wall to incident flux, evaluated as a function of the same variables.*

3.3. Stopping Power:

Analysis of the neutron energy spectra—both for particles re-entering the reactor core and those escaping through the rear wall (or transmitted neutrons, FIG 3, Bottom)—reveals a complex behavior. The transmitted neutron energy densities show a broad band starting between 100ev (d=0.5cm) and 10eV (d=20cm) and ending between 1.5MeV and 0.5MeV respectively, and then main peaks (in order of importance) at 14, 10, 1, 6 and 1.5 Mev. For these experiments, no significant effects are observed with the addition of Ti up to thicknesses greater than 3.5 cm. Beyond this, the increase in Ti shifts the maxima of the 100 Kev band to 10 Kev and reduces the size of the peaks above 1.5 MeV. This should favour the reaction Li6(n, α + T) over Li7(n, α + n' + T), but this has to be proven in further simulations considering the TBB attached to the plasma facing wall. Increasing the wall thickness shows a tendency to reduce the peaks above 1.5 MeV, increase those above 1 MeV, and shift the main band to lower energetic values. When analysing the spectra of recoil neutrons re-entering the nucleus, a well-differentiated band between 12eV and 3MeV is displayed (similar to the escaping neutron energy spectra), with a

well-differentiated minor peak in 1.5MeV and a wall length dependent main maximum in between 0.7MeV and 90KeV for 0.5 and 20 cm wall depth for pure Tungsten, respectively. Furthermore, the increase of Ti, for depths greater than 3.5 cm, tends to decrease the energy position of these main maxima and favors maxima at 10 keV.

Further examination of neutron fractions—those escaping toward the TBB (both interacting and non-interacting), re-entering the core, or absorbed within the wall —relative to the total source emission (Figure 3, Top) reveals

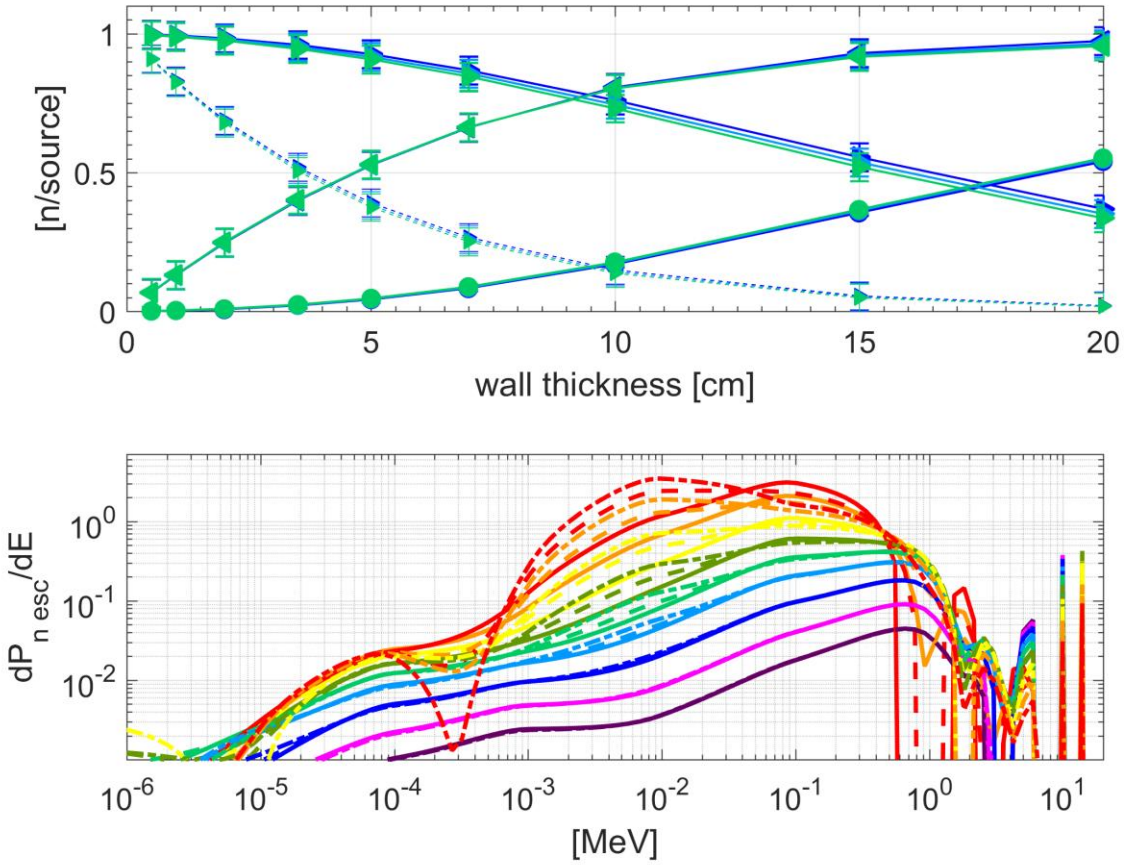

FIG.3. Top: *Representation of the shielding power of the wall, considering the incident neutrons that escape from the wall towards the TBB (ESC, forward triangle), is reflected in the core (nuc, reverse triangle) or are absorbed (fill circle). Dotted line represents the non-interacting wall particles that have escaped. Solid blue line for pure W, solid light blue line for 2% Ti and green line for 4% Ti alloy.* ***Bottom:*** *normalized energy spectrum distribution of the wall scaping neutrons (ESC). Solid line for pure W, dashed line for 2% Ti and dash-dot line for 4% Ti alloy.*

predominantly monotonic trends. Only the escaping fraction decreases with increasing thickness, while all other categories exhibit growth. Titanium appears to exert only a marginal influence, slightly increasing absorption and reducing all other reaction rates across all pathways.

3.4 Deposited Energy and DPA Rate:

Increasing the atomic fraction of titanium in the W-Ti alloy leads to a notable rise in energy deposition within the same material volume. Specifically, average increases of approximately 30±3% and 58±5% are observed for 2 wt.% and 4 wt.% Ti, respectively (FIG 1, bottom). Similarly, the corresponding displacement per atom (DPA) rates exhibit more pronounced increases of 34±5% and 70±10%, respectively (FIG 4). This agreement suggests that the presence of titanium may reduce the material's resistance to primary radiation damage.

With respect to wall thickness, both the deposited energy and DPA profiles exhibit Gaussian-like distributions (FIG 1, Bottom and figure 4 Top). The DPA peak values concentrated within the first 2.5 cm of depth. The position and magnitude of these maxima shifts asymptotically with increasing wall thickness. Notably, the peak in

deposited energy consistently occurs at a shallower depth than the DPA maximum, with its concentration within the first 7.5 mm of thickness.

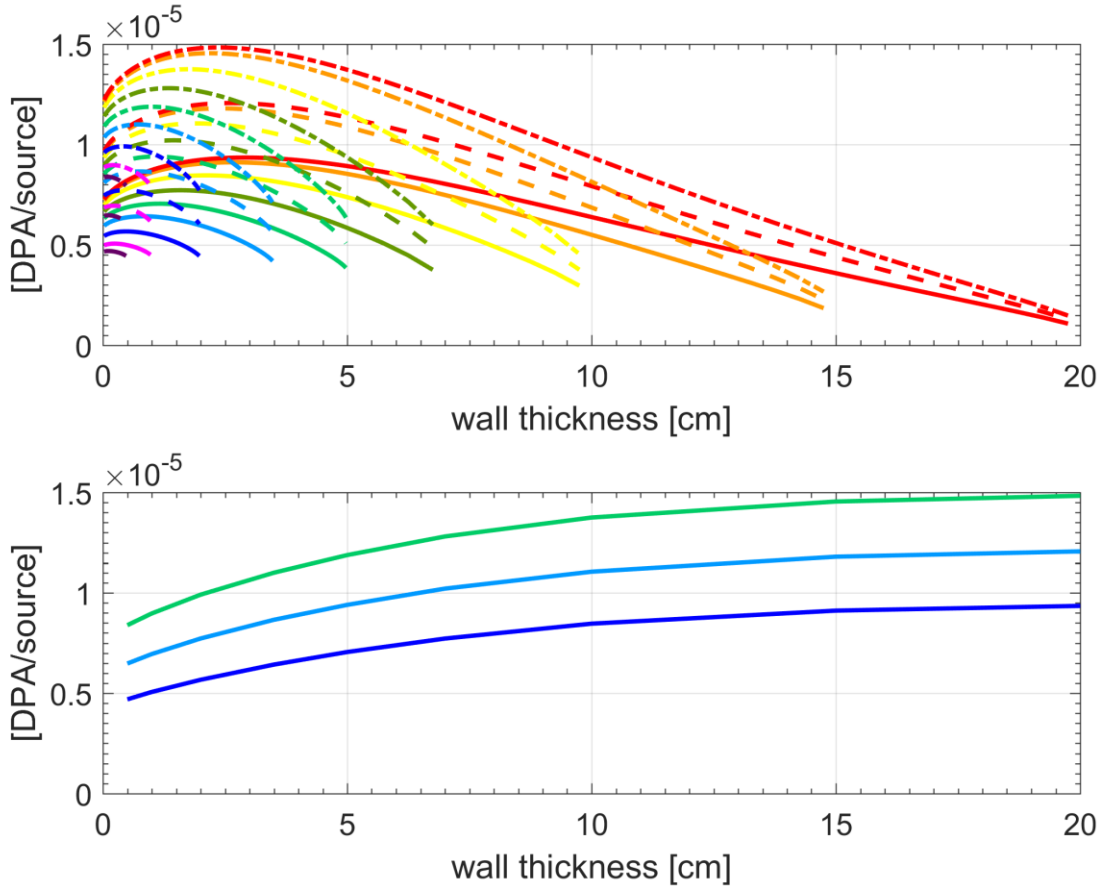

FIG. 4. ***Top:*** *Ti ratio and thickness-dependent DPA rate profile normalized to incident flux inside the wall.* ***Bottom****: Maximum value of DPA rate profile normalized to incident flux inside the wall vs wall depth. Solid blue line for pure W, solid light blue line for 2% Ti and green line for 4% Ti alloy.*

4. CONCLUSION

In this study, the neutron flux and the primary displacement damage rate (DPA/s) within the material were evaluated as a function of depth using MCNP5 radiation transport simulations. All results were normalized to the incident neutron flux, forming the foundation for a broader multiscale analysis.

The addition of titanium to tungsten has a negligible effect on neutron transport and multiplication. Both pure W and the W-Ti alloys exhibit strong neutron multiplication, with the (n,xn) reaction rate significantly exceeding absorption, maintaining the material's effectiveness as a neutron multiplier for fusion applications.

The inclusion of titanium shifts the neutron energy spectrum towards lower energies for thicker walls, especially for depths greater than 3.5 cm. This change is potentially beneficial for tritium breeding as it could favor the more efficient 6Li(n,α+T) reaction over the higher-energy 7Li(n,α+n′+T) reaction in an adjacent tritium breeding blanket. The findings suggest that while W-Ti alloys may offer certain engineering and neutron economy advantages, their performance under fusion neutron irradiation requires careful consideration due to the significantly increased primary damage and deposited energy.

The energy spectrum of neutrons exiting the structural wall—either toward the tritium breeding blanket (TBB) or re-entering the reactor core—was analysed in detail.

The findings indicate that wall thicknesses between 3.5 and 12 cm allow neutrons to escape with energy levels optimal for TBB performance, while the damage increase rate and net escaping / source neutron ratio gets into acceptable standards. The presence of titanium in the alloy does not significantly alter these energy characteristics.

Additionally, the energy distribution of neutrons escaping through the rear wall exhibits a bimodal pattern, with peaks above 12 MeV and between 0.5 and 3 MeV. Within the optimal thickness range, a slight increase in probability density is observed. The absence of neutrons in the intermediate energy band (5–10.5 MeV) may be attributed to the dominance of (n,xn) reactions over elastic scattering, while the high-energy peak likely results from secondary neutron production via (n,2n) and (n,3n) reactions.

To accurately assess the net material degradation and determine whether titanium significantly influences primary damage mechanisms, it is essential to complement these findings with molecular dynamics simulations. This next phase of the research will build upon the data generated in the current study, enabling a more comprehensive understanding of radiation-induced damage at the atomistic level.

ACKNOWLEDGEMENTS

A.Z. wishes to thank C. Pastorino for image formatting, J. Torres and B. Bruzzo for technical support in the SOL67 supercomputing node in CAC, J. Gallardo for his assistance on MCNP5 coding, Conicet and CNEA for the doctoral scholarship, the Instituto Sabato and the University of San Martin.

REFERENCES

[1] Ohr, K. & Jr, R. & Barker, D. "The effective use of tungsten as a shielding material in nuclear applications". 2003 International ISOE ALARA Symposium, January 15, 2003, Orlando, Florida, USA. 46. 45-48.
[2] J.A. GARCIA GALLARDO1, M.A.N. GIMENEZ, J. L. GERVASONI, "nuclear properties of tungsten under 14 MeV neutron irradiation for fusion-fission hybrid reactors", Annals of Nuclear Energy, Volume 147, November 2020, 107739
[3] D.Y. Jianga et al., "Mechanical properties of W–Ti alloys from first-principles calculations, Fusion Engineering and Design" 106 (2016) 34–39
[4] Z. Cao, M. Pan, K. Hu, "Effect of titanium on the precipitation behaviors of transmutation elements in tungsten-titanium alloys from first-principles calculations", Fusion Engineering and Design 158 (2020) 111673.
[5] C.J.W. Cook, T. Schöberl, A.S.G.K. Singh, D.F. Bahr, "Properties of Mechanically Alloyed W-Ti Materials with Dual Phase Particle Dispersion", Materials 10(12) (2017) 1438.
[6] M.R. Gilbert, J.P.H. Mason, L. Packer, "Neutron-induced transmutation effects in W and W-alloys in a fusion environment", Fusion Engineering and Design 88(6-8) (2013) 1251–1254.
[7] Xunxiang Hu; "Recent progress in experimental investigation of neutron irradiation response of tungsten"; Journal of Nuclear Materials 568, (2022), 153856
[8] S. Chen, "Calculation and verification of neutron irradiation damage with differential cross sections, Nuclear Materials and Energy", 28, 101284 (2022).
[9] A.Yu. Konobeyev et al.; "Evaluation of effective threshold displacement energies and other data required for the calculation of advanced atomic displacement cross-sections"; Nuclear Energy and Technology 3 (2017) 169–175.
[10] A. A. Fierro Rodriguez, "Sistema de frenado de neutrones y reproducción de tritio en plantas de fusión nuclear por confinamiento inercial"; (2020) Tesis doctoral, Universidad Politécnica de Madrid.
[11] M.T. Robinson, I.M. Torrens, "Computer simulation of atomic-displacement cascades in solids in the binary-collision approximation", Phys. Rev. B. 9 (1974) 5008–5024, https://doi.org/10.1103/PhysRevB.9.5008
[12] A.Y. Konobeyev, U. Fischer, P.E. Pereslavtsev, "Evaluation of advanced displacement cross-sections for the major EUROFER constituents based on an atomistic modelling approach", Kerntechnik. 80 (2015) 7–12, https://doi.org/10.3139/124.110483.
[13] K. Nordlund, S.J. Zinkle, A.E. Sand, F. Granberg, R.S. Averback, R.E. Stoller, T. Suzudo, L. Malerba, F. Banhart, W.J. Weber, F. Willaime, S.L. Dudarev, D. Simeone, "Primary radiation damage: A review of current understanding and models", J. Nucl. Mater. 512 (2018) 450–479, https://doi.org/10.1016/j.jnucmat.2018.10.027.
[14] K. Nordlund, A.E. Sand, F. Granberg, S.J. Zinkle, R.E. Stoller, R.S. Averback, T. Suzudo, L. Malerba, F. Banhart, W.J. Weber, F. Willaime, S.L. Dudarev, D. Simeone, "Primary Radiation Damage in Materials", OECD/NEA (2015).
[15] K. Nordlund, S.J. Zinkle, A.E. Sand, F. Granberg, R.S. Averback, R. Stoller, T. Suzudo, L. Malerba, F. Banhart, W.J. Weber, F. Willaime, S.L. Dudarev, D. Simeone, "Improving atomic displacement and replacement calculations with physically realistic damage models", Nat. Commun. 9 (2018) 1084, https://doi.org/10.1038/s41467-018-03415-5.
[16] S. Chen, "Calculation and verification of neutron irradiation damage with differential cross sections", Nuclear Materials and Energy, 28, 101284 (2022).